ADVANCED MATERIALS

Supporting Information

for *Adv. Mater.*, DOI: 10.1002/adma.201400058

High-Performance Pseudocubic Thermoelectric Materials from Non-cubic Chalcopyrite Compounds

Jiawei Zhang, Ruiheng Liu, Nian Cheng, Yubo Zhang, Jihui Yang, Ctirad Uher, Xun Shi, Lidong Chen*, and Wenqing Zhang**

Submitted to ADVANCED MATERIALS

Supporting information for

High-performance Pseudocubic Thermoelectric Materials from Non-cubic Chalcopyrite Compounds

By Jiawei Zhang[1,2], Ruiheng Liu[1], Nian Cheng[1,2], Yubo Zhang[1], Jihui Yang[3], Ctirad Uher[4], Xun Shi[1], Wenqing Zhang[1*], and Lidong Chen[1*]*

Mr. Jiawei Zhang, Dr. Ruiheng Liu, Mr. Nian Cheng, Dr. Yubo Zhang, Prof. Xun Shi, Wenqing Zhang, Lidong Chen
State Key Laboratory of High Performance Ceramics and Superfine Microstructure, Shanghai Institute of Ceramics, Chinese Academy of Sciences, 1295 Dingxi Road, Shanghai 200050, China.
E-mail: xshi@mail.sic.ac.cn; wqzhang@mail.sic.ac.cn; cld@mail.sic.ac.cn

Mr. Jiawei Zhang and Nian Cheng
University of Chinese Academy of Sciences, Beijing 100049, China.

Prof. Jihui Yang
Materials Science and Engineering Department, University of Washington, Seattle, Washington 98195-2120, USA

Prof. Ctirad Uher
Department of Physics, University of Michigan, Ann Arbor, Michigan 48109, USA.

Keywords: thermoelectric, pseudocubic structure, non-cubic compounds, degenerate electronic bands

This supporting information includes:

Crystal field splitting in tetragonal chalcopyrite compounds

Schematic map of electronic bands in tetragonal chalcopyrites is exemplified in **Figure S1**. Δ_{CF}, the crystal field splitting parameter, is defined as the energy difference between Γ_{5v} and Γ_{4v}. Typical tetragonal chalcopyrites, including $CuInTe_2$, $CuGaTe_2$, $AgGaTe_2$, $AgInSe_2$, ST-$Cu_2ZnSnSe_4$, ST-Cu_2ZnSnS_4 and ST-$Cu_2ZnGeSe_4$, are studied and discussed in this work.

Calculation details of solid solutions

Solid solution calculations are carried out in a supercell with 64 atoms (2×2×1 unit cell). Considering the computational cost, here we use PBE+U method for crystal structure optimization. We take $CuIn_xGa_{1-x}Te_2$ as an example. There are 16 equivalent positions for Ga/In atoms, thus the possible atomic concentrations of In are multiples of 1/16.The crystal structure of the supercell with the lowest energy is used for further calculations and analysis. In the range of the crystal distortion parameters close to unity, the total energy difference between those possible solution structures is small. Error bars for crystal field splitting and structure distortion are also given in **Figure S8** (see below).

X-ray Diffraction

X-ray powder diffraction patterns of $Cu_{1-x}Ag_xInTe_2$ are shown in **Figure S2**. The calculated lattice parameters are shown in **Figure S3**. Lattice parameters *a* and *c* increase linearly when the doping concentration of Ag (*x*) increases. The lattice parameters of $Cu_{1-x}Ag_xInTe_2$ follow the linear curve between $CuInTe_2$ and $AgInTe_2$, obeying well the Vegard's law. This indicates that solid solutions between $CuInTe_2$ and $AgInTe_2$ are formed when *x* is less than 0.2.

Theoretical power factors and their dependence on crystal field splitting

Electrical transport property calculations for all compounds were carried out by combining the *ab initio* band structure calculations and the Boltzmann transport theory under the constant electron relaxation time approximation. Methodology framework and computational details were presented in Refs. 1-3. In brief, a full band approximation was used to calculate electron group velocity and density of electron states,[1] and a very dense 21×21×21 *k* mesh was used to get converged transport properties. This approach has been successfully used to estimate the Seebeck coefficients and evaluate the electrical conductivities and power factors, including their dependence on doping or carrier concentrations and temperature, for many thermoelectric compounds including different chalcopyrite compounds before.[1-3]

The crystal field splitting energy Δ_{CF} was varied by slightly tuning crystal distortion parameter η. Considering the relatively minor changes to the crystal structure for each step, the electron relaxation time τ was approximated to be independent of Δ_{CF} in the current work. For each Δ_{CF} value, the theoretical maximum power factor $\sigma S^2/\tau$ was evaluated and plotted in Figure S5.

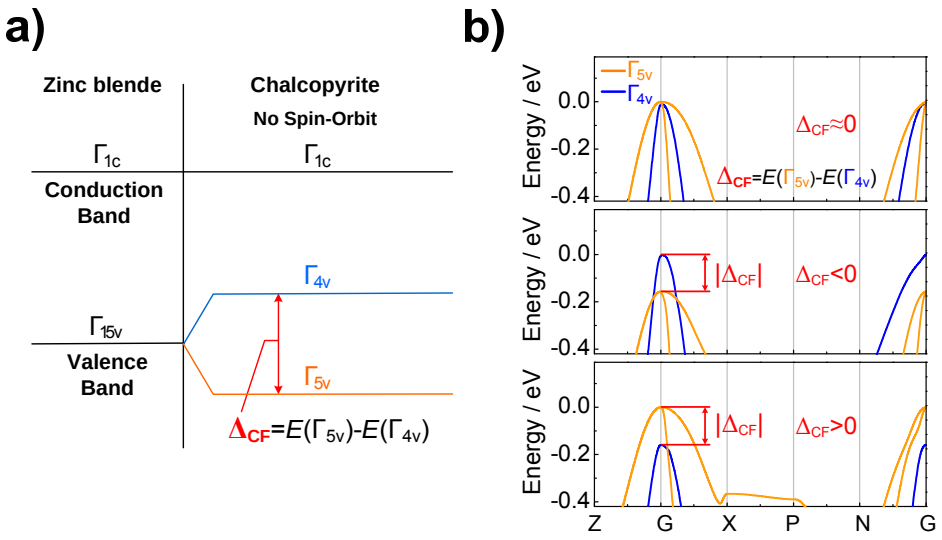

Figure S1. Non-cubic characteristics in tetragonal chalcopyrites due to crystal field effect. a) Crystal field splitting in ternary chalcopyrite compounds. b) Calculated electronic bands for non-cubic tetragonal chalcopyrites with zero (the top one) and non-zero Δ_{CF} values.

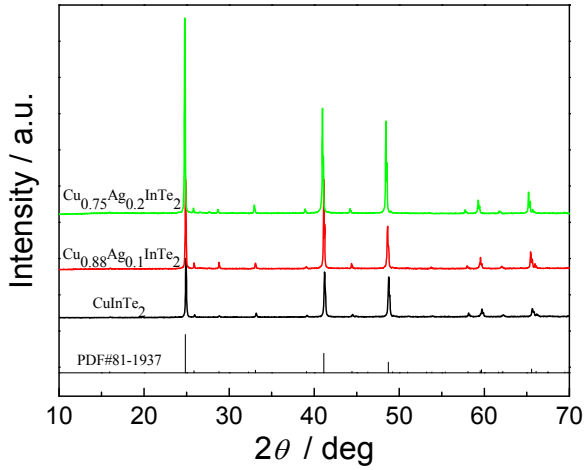

Figure S2. X-ray powder diffraction patterns of $Cu_{1-x}Ag_xInTe_2$.

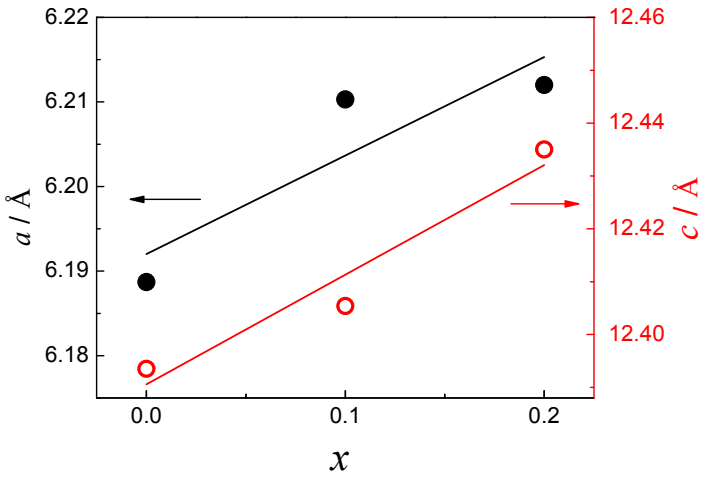

Figure S3. Calculated experimental lattice parameters *a* and *c* for $Cu_{1-x}Ag_xInTe_2$ based on the measured X-ray diffraction patterns.

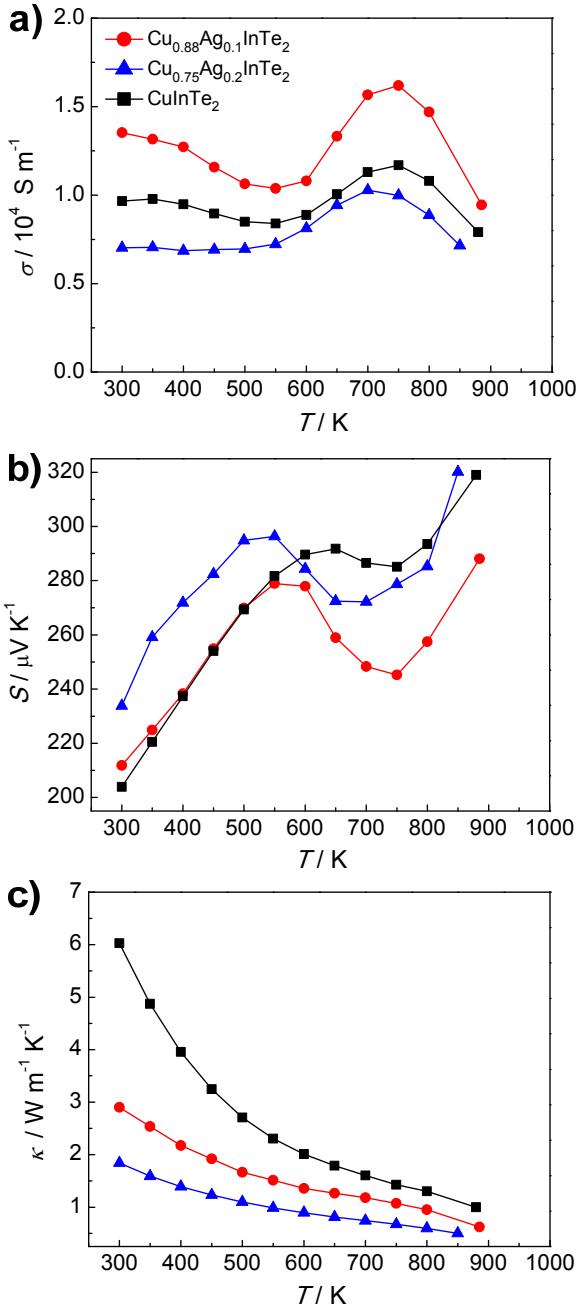

Figure S4. Temperature dependent electrical conductivity(σ) (a), thermopower (S) (b), and thermal conductivity (κ) (c) of $Cu_{1-x}Ag_xInTe_2$.

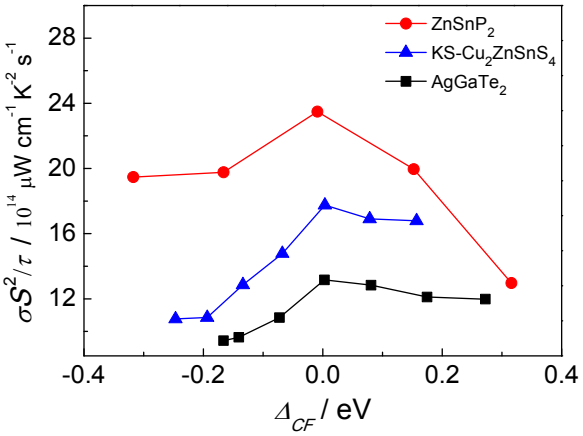

Figure S5. Calculated $\sigma S^2/\tau$ as a function of Δ_{CF} in tetragonal chalcopyrite compounds.

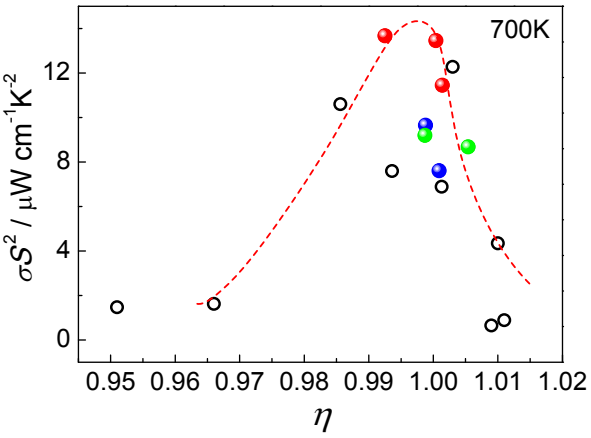

Figure S6. Experimental power factors[4-12] at 700K as a function of η in chalcopyrite compounds. Similar to **Figure 3**, the power factors of compounds with η around 1 show obviously higher values. A value around zero for Δ_{CF} (or 1 for η) leads to high power factors as well as high thermoelectric performance.

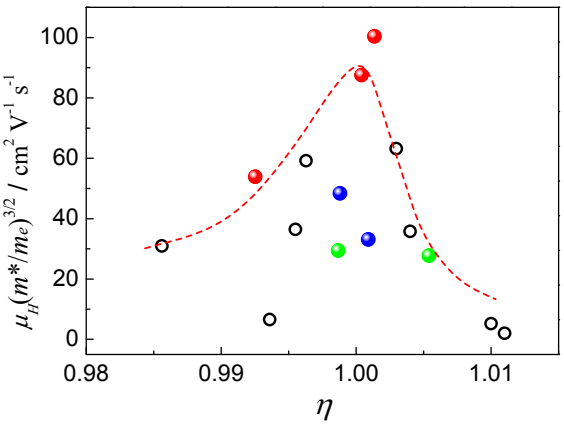

Figure S7. Experimental $\mu_H(m^*/m_e)^{3/2}$ at room temperature as a function of η in chalcopyrites. The $\mu_H(m^*/m_e)^{3/2}$ values are calculated based on our experimental data and references[4,6,7,10,12-14] using the single parabolic band approximation as well as acoustic phonon scattering to carriers. Compounds with zT values above 1 are marked in red. The blue (or green) points represent mixtures or solid solutions between $AgInTe_2$ (or $CuGaTe_2$) and $CuInTe_2$.

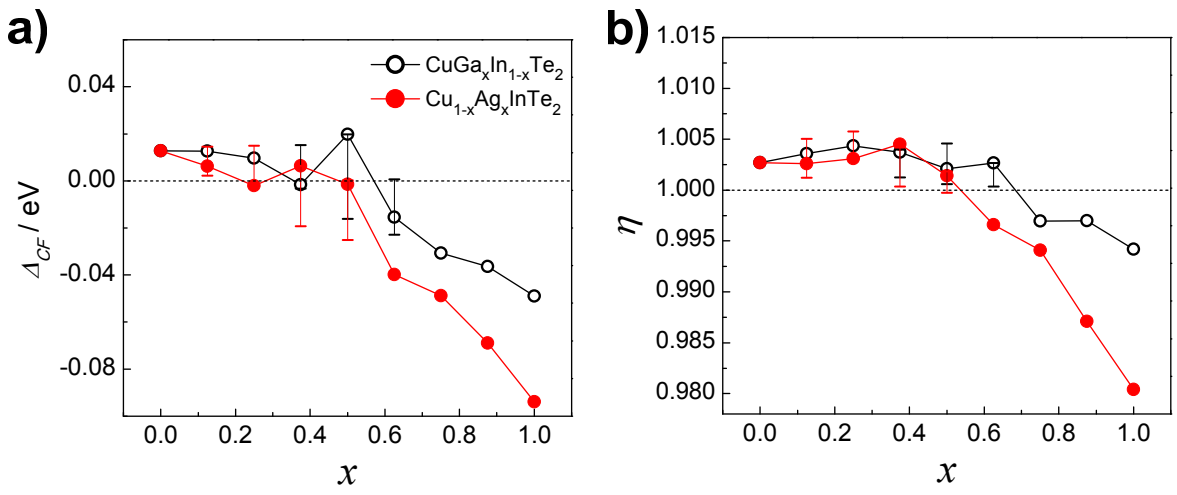

Figure S8. Calculated Δ_{CF} (a) and η (b) as a function of x in $CuGa_xIn_{1-x}Te_2$ and $Cu_{1-x}Ag_xInTe_2$. Error bars for compositions with Δ_{CF} around zero and η around 1 are shown in the figure.

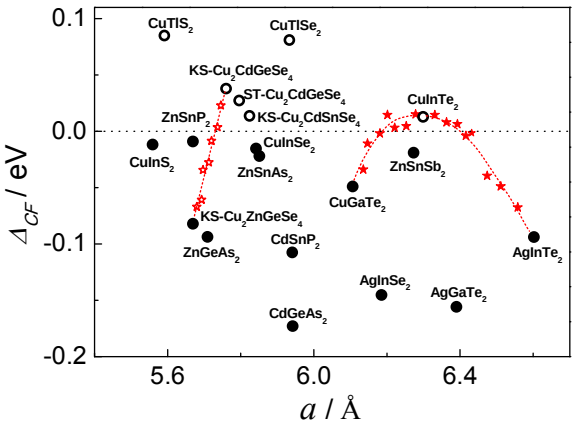

Figure S9. Tetragonal crystal field splitting Δ_{CF} as a function of lattice constant a in chalcopyrites with E_g < 1.7eV. The red stars with trend line represent mixtures or solid solutions between two chalcopyrite compounds with positive and negative Δ_{CF} values. The dotted line is the zero line. Filled circles are negative Δ_{CF} compounds. Empty circles are positive Δ_{CF} compounds. ST and KS represent stannite structure and kesterite structure, respectively.

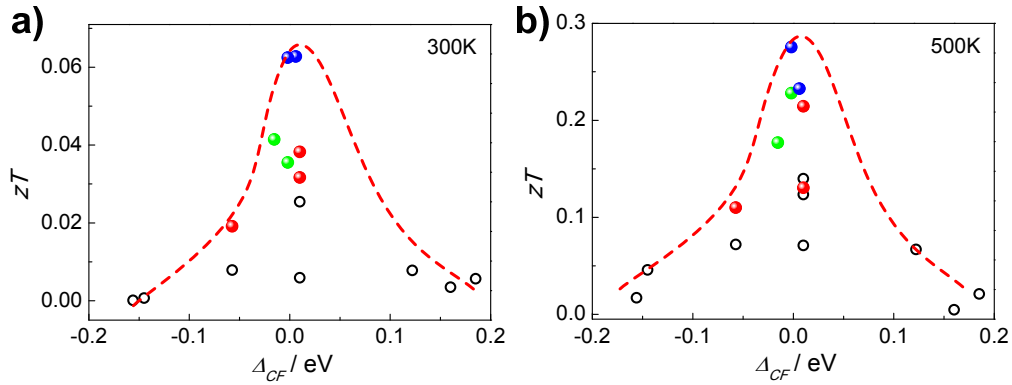

Figure S10. Experimental zT values[4-12] at 300 K (a) and 500 K (b) as a function of Δ_{CF} in chalcopyrite compounds.

Table S1. Calculated lattice parameters, crystal field splitting energy, and energy gaps of tetrahedral chalcopyrites. Potential TE compounds are marked in red color. Δ_{CF}^{exp} and E_g^{exp} represent experimental crystal field splitting energy and experimental band gap respectively. The band gaps of KS-I_2-II-IV-VI_4 are calculated values. KS means kesterite structure. The method for the calculation of anion displacement is given in ref. 35 in the main text. For the compounds of Cu_3SbSe_4, $CuTlSe_2$, $CuTlS_2$, $CdSnAs_2$, $ZnSnSb_2$ and $CdSnSb_2$, we used mBJ+U method[15,16] in WIEN2k[17] to calculate the electronic structures.

I-III-VI_2 Chalcopyrites						
Compounds	a (Å)	η	u	Δ_{CF} (eV)	Δ_{CF}^{exp} (eV)	E_g^{exp} (eV)
$AgAlS_2$	5.743	0.902	0.297	-0.252		3.13[18]
$AgAlSe_2$	6.017	0.912	0.289	-0.300		2.55[18]
$AgAlTe_2$	6.394	0.947	0.274	-0.164		2.27[18]
$AgGaS_2$	5.785	0.903	0.290	-0.255	-0.28[18]	2.7[18]
$AgGaSe_2$	6.034	0.918	0.283	-0.230	-0.25[18]	2.29[18]
$AgGaTe_2$	6.390	0.951	0.271	-0.156		1.32[18]
$AgInS_2$	5.929	0.963	0.263	-0.158	-0.15[18]	1.87[18]
$AgInSe_2$	6.185	0.966	0.259	-0.145	-0.12[18]	1.24[18]
$AgInTe_2$	6.551	0.981	0.249	-0.090		1.12[18]
$CuAlS_2$	5.333	0.981	0.262	-0.163	-0.13[18]	3.49[18]
$CuAlSe_2$	5.637	0.979	0.258	-0.145	-0.17[18]	2.65[18]
$CuAlTe_2$	6.078	0.989	0.246	-0.078		2.06[18]
$CuGaS_2$	5.366	0.983	0.254	-0.125	-0.12[18]	2.43[18]
$CuGaSe_2$	5.652	0.984	0.251	-0.109	-0.09[18]	1.68[18]
$CuGaTe_2$	6.071	0.992	0.243	-0.057	-0.08[18]	1.23[19]
$CuInS_2$	5.559	1.010	0.226	-0.012	>-0.005[18]	1.53[20]
$CuInSe_2$	5.842	1.006	0.225	-0.015	0.006[18]	1.04[21]
$CuInTe_2$	6.247	1.004	0.222	0.010	0[18]	0.98[22]
$CuTlSe_2$	5.933	1.005	0.209	0.081		
$CuTlS_2$	5.591	1.001	0.190	0.085		1.39[18]
II-IV-VI_2 Chalcopyrites						
$CdGeP_2$	5.767	0.941	0.284	-0.1982	-0.2[18]	1.72[18]
$CdSiAs_2$	5.928	0.924	0.291	-0.2525	-0.24[18]	1.55[18]
$CdSiP_2$	5.693	0.919	0.298	-0.2459	-0.2[18]	2.75[18]
$MgSiP_2$	5.709	0.889	0.293	-0.2917		2.82[18]
$ZnSiP_2$	5.397	0.969	0.270	-0.1276	-0.12[18]	2.98[18]
$ZnGeP_2$	5.475	0.982	0.257	-0.0844	-0.08[18]	1.92[18]
$ZnSiAs_2$	5.633	0.971	0.266	-0.1324	-0.13[18]	2.12[18]
$CdGeAs_2$	5.942	0.944	0.287	-0.173	-0.21[18]	0.57[18]
$CdSnP_2$	5.941	0.976	0.260	-0.108	-0.1[18]	1.17[18]
$CdSnSb_2$	6.479	0.985	0.240	-0.093		0.16[18]
$ZnGeAs_2$	5.709	0.983	0.254	-0.094	-0.06[18]	1.15[18]

$CdSnAs_2$	6.158	0.977	0.244	-0.12	-0.06[18]	0.26[18]
$ZnSnAs_2$	5.890	1.001	0.270	-0.02	0[18]	0.745[18]
$ZnSnSb_2$	6.345	1.001	0.273	-0.02		0.4[18]
$ZnSnP_2$	5.669	1.001	0.232	-0.009	0[18]	1.66[18]
			I_2-II-IV-VI_4			
KS-$Cu_2CdGeSe_4$	5.722	1.002	0.239	0.051		1.16[23]
ST-$Cu_2CdGeSe_4$	5.801	0.961	0.235	0.019		1.2[24]
KS-Cu_2CdSnS_4	5.539	1.012	0.228	0.023		1.41[23]
ST-Cu_2CdSnS_4	5.614	0.971	0.228	-0.019		1.37[25]
KS-$Cu_2CdSnSe_4$	5.824	1.006	0.227	0.014		0.85[23]
ST-$Cu_2CdSnSe_4$	5.882	0.976	0.226	0.02		0.98[26]
KS-$Cu_2ZnGeSe_4$	5.642	0.986	0.251	-0.077		1.33[23]
ST-$Cu_2ZnGeSe_4$	5.585	1.011	0.248	0.185		1.63[24]
KS-Cu_2ZnSnS_4	5.448	0.998	0.242	-0.065		1.65[23]
ST-Cu_2ZnSnS_4	5.424	1.009	0.239	0.16		1.5[27]
KS-$Cu_2ZnSnSe_4$	5.727	0.997	0.239	-0.048		1.08[23]
ST-$Cu_2ZnSnSe_4$	5.699	1.010	0.238	0.122		1.44~1.5[28]

Table S2. Experimental lattice parameters and room temperature thermoelectric transport properties of tetrahedral chalcopyrite compounds. The red color represents calculated values. ST means stannite structure.

Systems	η	S ($\mu V\ K^{-1}$)	p ($10^{20}\ cm^{-3}$)	μ_H ($cm^2\ V^{-1}\ s^{-1}$)	m^*/m_e	$\mu_H(m^*/m_e)^{3/2}$ ($cm^2\ V^{-1}\ s^{-1}$)
$CuInTe_2$[7]	1.0004	254	0.106	85	1.02	87.56
$CuInTe_2$[7]	1.0014	384	0.0187	117	0.90	100.40
$CuInTe_2$[7]	1.0030	273	0.0575	90	0.79	63.20
$CuInTe_2$[6]	1.0040	425.7	0.0043	111	0.47	35.77
$CuInTe_2$	1.0013	203.9	0.1237	48.8	0.742	31.19
$Ag_{0.1}Cu_{0.88}InTe_2$	0.9988	211.8	0.1899	44.53	1.057	48.39
$Ag_{0.2}Cu_{0.75}InTe_2$	1.0009	233.9	0.133	32.93	1.004	33.13
$Ag_{0.3}Cu_{0.68}InTe_2$	0.9955	256.38	0.1169	31.22	1.109	36.46
$CuGaTe_2$(318K)[12]	0.9936	134.6	0.205	17.5	0.52	6.56
$CuGaTe_2$[4]	0.9925	380	0.011	112	0.61	53.89
Cu_3SbSe_4[13]	0.9963	472.9	0.004	114	0.65	59.19
ST-$Cu_2ZnSnSe_4$[10]	1.010	130	0.1	28.13	0.33	5.24
ST-$Cu_2ZnGeSe_4$(360K)[14]	1.011	315.8	0.0214	6.06	0.48	2.02
$CuIn_{0.36}Ga_{0.64}Te_2$[12]	1.0054	365	0.0504	16.4	1.42	27.75
$CuIn_{0.64}Ga_{0.36}Te_2$[12]	0.9987	391	0.0537	12	1.82	29.46

Table S3. Calculated bond lengths and anion displacements of $Cu_{0.875}Ag_{0.125}InTe_2$ and $Cu_{0.75}Ag_{0.25}InTe_2$. Anion displacements are calculated using $u = 0.25 + \frac{(R^2_{[Cu(Ag)\text{-}Te]\text{-}1} + R^2_{[Cu(Ag)\text{-}Te]\text{-}2}) - (R^2_{[In\text{-}Te]\text{-}1} + R^2_{[In\text{-}Te]\text{-}2})}{2a^2}$.

Bond length				u
[Cu(Ag)-Te]-1	[Cu(Ag)-Te]-2	[In-Te]-1	[In-Te]-2	
$CuInTe_2$				
2.611	2.611	2.815	2.815	0.222
$AgInTe_2$				
2.816	2.816	2.823	2.823	0.249
$Cu_{0.875}Ag_{0.125}InTe_2$				
2.624	2.632	2.868	2.872	0.217
2.624	2.625	2.869	2.871	0.216
2.613	2.628	2.847	2.859	0.218
2.615	2.791	2.851	2.845	0.230
$Cu_{0.75}Ag_{0.25}InTe_2$				
2.622	2.815	2.850	2.849	0.232
2.610	2.813	2.857	2.850	0.231
2.622	2.814	2.852	2.851	0.232
2.626	2.637	2.865	2.860	0.219
2.604	2.813	2.849	2.861	0.230
2.628	2.627	2.860	2.869	0.218
2.626	2.619	2.858	2.874	0.217
2.626	2.620	2.860	2.877	0.217

Reference

[1] J. Yang, H. Li, T. Wu, W. Zhang, L. Chen, J. Yang, *Adv. Funct. Mater.* **2008**, *18*, 2880.

[2] a) D. Singh, *Phys. Rev. B* **2010**, *81*, 195217; b) D. Parker, D. J. Singh, *Phys. Rev. B* **2012**, *85,* 125209; c) L. L. Xi, Y. B. Zhang, X. Y. Shi, J. Yang, X. Shi, L. D. Chen, W. Zhang, *Phys. Rev. B* **2012**, *86*, 155201; d) J. Yang, P. Qiu, R. Liu, L. Xi, S. Zheng, W. Zhang, L. Chen, D. J. Singh, J. H. Yang, *Phys. Rev. B* **2011**, *84*, 235205.

[3] G. K. H. Madsen, D. J. Singh, *Comput. Phys. Commun.* **2006**, *175*, 67.

[4] T. Plirdpring, K. Kurosaki, A. Kosuga, T. Day, S. Firdosy, V. Ravi, G. J. Snyder, A. Harnwunggmoung, T. Sugahara, Y. Ohishi, H. Muta, S. Yamanaka, *Adv. Mater.* **2012**, *24*, 3622.

[5] M. Ibanez, R. Zamani, A. LaLonde, D. Cadavid, W. Li, A. Shavel, J. Arbiol, J. R. Morante, S. Gorsse, G. J. Snyder, A. Cabot, *J. Am. Chem. Soc.* **2012**, *134*, 4060.

[6] A. Kosuga, T. Plirdpring, R. Higashine, M. Matsuzawa, K. Kurosaki, S. Yamanaka, *Appl. Phys. Lett.* **2012**, *100*, 042108.

[7] R. Liu, L. Xi, H. Liu, X. Shi, W. Zhang, L. Chen, *Chem. Commun.* **2012**, *48*, 3818.

[8] P. Z. Ying, H. Zhou, Y. L. Gao, Y. Y. Li, Y. P. Li, X. L. Lian, J. L. Cui, *Key Eng. Mater.* **2012**, *519*, 188.

[9] A. Yusufu, K. Kurosaki, A. Kosuga, T. Sugahara, Y. Ohishi, H. Muta, S. Yamanaka, *Appl. Phys. Lett.* **2011**, *99*, 061902.

[10] X. Y. Shi, F. Q. Huang, M. L. Liu, L. D. Chen, *Appl. Phys. Lett.* **2009**, *94*, 122103.

[11] M. L. Liu, F. Q. Huang, L. D. Chen, I. W. Chen, *Appl. Phys. Lett.* **2009**, *94*, 202103.

[12] Y. Li, Q. Meng, Y. Deng, H. Zhou, Y. Gao, Y. Li, J. Yang, J. Cui, *Appl. Phys. Lett.* **2012**, *100*, 231903.

[13] C. Yang, F. Huang, L. Wu, K. Xu, *J. Phys. D: Appl. Phys.* **2011**, *44*, 295404.

[14] W. G. Zeier, A. LaLonde, Z. M. Gibbs, C. P. Heinrich, M. Panthoefer, G. J. Snyder, W. Tremel, *J. Am. Chem. Soc.* **2012**, *134*, 7147.

[15] F. Tran, P. Blaha, *Phys. Rev. Lett.* **2009**, *102*, 226401.

[16] Y. Zhang, J. Zhang, W. Gao, T. A. Abtew, Y. Wang, P. Zhang, W. Zhang, *J. Chem. Phys.* **2013**, *139*, 184706.

[17] K. Schwarz, P. Blaha, *Comp. Mater. Sci.* **2003**, *28*, 259.

[18] L. I. Berger, *Semiconductor Materials* , CRC Press**, 1997**.

[19] H. Neumann, W. Horig, E. Reccius, H. Sobotta, B. Schumann, G. Kuhn, *Thin Solid Films* **1979**, *61*, 13.

[20] B. Tell, J. L. Shay, H. M. Kasper, *Phys. Rev. B* **1971**, *4*, 2463.

[21] J. L. Shay, B. Tell, H. M. Kasper, L. M. Schiavone, *Phys. Rev. B* **1973**, *7*, 4485.

[22] T. Ishizaki, N. Saito, A. Fuwa, *Surf. Coat. Tech.* **2004**, *182*, 156.

[23] Y. B. Zhang, X. D. Sun, P. H. Zhang, X. Yuan, F. Q. Huang, W. Q. Zhang, *J. Appl. Phys.* **2012**, *111*, 063709.

[24] H. Matsushita, T. Maeda, A. Katsui, T. Takizawa, *J. Cryst. Growth* **2000**, *208*, 416.

[25] H. Matsushita, T. Ichikawa, A. Katsui, *J. Mater. Sci.* **2005**, *40*, 2003.

[26] M. L. Liu, I. W. Chen, F. Q. Huang, L. D. Chen, *Adv. Mater.* **2009**, *21*, 3808.

[27] H. Katagiri, *Thin Solid Films* **2005**, *480*, 426.

[28] R. A. Wibowo, E. S. Lee, B. Munir, K. H. Kim, *Phys. Status Solidi A* **2007**, *204*, 3373.